

Light harvesting with Ge quantum dots embedded in SiO₂ or Si₃N₄

Salvatore Cosentino, Emel Sungur Ozen, Rosario Raciti, Antonio M. Mio, Giuseppe Nicotra, Francesca Simone, Isodiana Crupi, Rasit Turan, Antonio Terrasi, Atilla Aydinli, and Salvo Mirabella

Citation: *Journal of Applied Physics* **115**, 043103 (2014); doi: 10.1063/1.4863124

View online: <http://dx.doi.org/10.1063/1.4863124>

View Table of Contents: <http://scitation.aip.org/content/aip/journal/jap/115/4?ver=pdfcov>

Published by the AIP Publishing

Articles you may be interested in

[Determining the crystalline degree of silicon nanoclusters/SiO₂ multilayers by Raman scattering](#)

J. Appl. Phys. **115**, 203504 (2014); 10.1063/1.4878175

[Photoluminescence properties and crystallization of silicon quantum dots in hydrogenated amorphous Si-rich silicon carbide films](#)

J. Appl. Phys. **115**, 164303 (2014); 10.1063/1.4871980

[Amorphous Ge quantum dots embedded in Si O 2 formed by low energy ion implantation](#)

J. Appl. Phys. **103**, 124304 (2008); 10.1063/1.2927254

[Quantum confinement of E 1 and E 2 transitions in Ge quantum dots embedded in an Al 2 O 3 or an AlN matrix](#)

Appl. Phys. Lett. **76**, 43 (2000); 10.1063/1.125650

[A comparative study of Ge nanocrystals in Si x Ge y O z alloys and SiO x /GeO y multilayers](#)

J. Appl. Phys. **81**, 2384 (1997); 10.1063/1.364242

Frustrated by old technology? Is your AFM dead and can't be repaired? Sick of bad customer support?



It is time to upgrade your AFM
Minimum \$20,000 trade-in discount for purchases before August 31st

Asylum Research is today's technology leader in AFM

dropmyoldAFM@oxinst.com

OXFORD INSTRUMENTS
The Business of Science®

Light harvesting with Ge quantum dots embedded in SiO₂ or Si₃N₄

Salvatore Cosentino,^{1,a)} Emel Sungur Ozen,² Rosario Raciti,¹ Antonio M. Mio,³ Giuseppe Nicotra,³ Francesca Simone,¹ Isodiana Crupi,¹ Rasit Turan,⁴ Antonio Terrasi,¹ Atila Aydinli,² and Salvo Mirabella¹

¹MATIS IMM-CNR and Dipartimento di Fisica e Astronomia, Università di Catania, via S. Sofia 64, 95123 Catania, Italy

²Department of Physics, Bilkent University, 06800 Ankara, Turkey

³IMM-CNR, VII strada 5, 95121 Catania, Italy

⁴Department of Physics, Middle East Technical University, 06531 Ankara, Turkey

(Received 17 October 2013; accepted 12 January 2014; published online 27 January 2014)

Germanium quantum dots (QDs) embedded in SiO₂ or in Si₃N₄ have been studied for light harvesting purposes. SiGeO or SiGeN thin films, produced by plasma enhanced chemical vapor deposition, have been annealed up to 850 °C to induce Ge QD precipitation in Si based matrices. By varying the Ge content, the QD diameter can be tuned in the 3–9 nm range in the SiO₂ matrix, or in the 1–2 nm range in the Si₃N₄ matrix, as measured by transmission electron microscopy. Thus, Si₃N₄ matrix hosts Ge QDs at higher density and more closely spaced than SiO₂ matrix. Raman spectroscopy revealed a higher threshold for amorphous-to-crystalline transition for Ge QDs embedded in Si₃N₄ matrix in comparison with those in the SiO₂ host. Light absorption by Ge QDs is shown to be more effective in Si₃N₄ matrix, due to the optical bandgap (0.9–1.6 eV) being lower than in SiO₂ matrix (1.2–2.2 eV). Significant photoresponse with a large measured internal quantum efficiency has been observed for Ge QDs in Si₃N₄ matrix when they are used as a sensitive layer in a photodetector device. These data will be presented and discussed, opening new routes for application of Ge QDs in light harvesting devices. © 2014 AIP Publishing LLC. [<http://dx.doi.org/10.1063/1.4863124>]

INTRODUCTION

In the past decade, group-IV nanostructures (NS) received much attention as new material for efficient optoelectronic devices,^{1,2} photodetectors,^{3,4} and solar cells.^{5,6} In particular, Ge nanostructures gained a renewed interest because of their larger absorption, stronger quantum confinement effect (QCE) due to the larger Bohr radius (~24 nm)^{7,8} and lower synthesis temperature in comparison with Si nanostructures. The exploitation of these properties and their application for efficient light harvesting devices have been quite extensively studied in recent years. Ge quantum dots (QDs) in SiO₂ have been already used for the fabrication of QD-based memories,⁹ efficient light harvesters,^{2,3,10} or for the application in novel multi-junction solar cells.^{6,11} However, the optical behavior and the band-gap tuning of Ge QDs does not depend on QD size only, as a basic confinement effect rule predicts. Other effects have been demonstrated to have a strong role in the light absorption/emission process such as: mid-gap states and defects at the interface with the matrix,^{12–14} crystallinity (amorphous (a-) or crystalline (c-)) of QDs,¹⁵ the shape of the QDs and their size distribution,^{16,17} as well as the nature of the surrounding matrix.¹⁸ However, one of the main problems with quantum dots embedded in dielectrics is the poor extraction of photo-generated carriers. Compared with silicon dioxide (SiO₂), silicon nitride (Si₃N₄) matrix can be a promising new host matrix for QDs. In fact, the lower barrier height offered

by Si₃N₄ can ensure better carrier transport and extraction mechanism in QD-based devices, while continuing to preserve the control of the band-gap tuning through QCE. However, only few studies have been performed in the past on Ge QDs embedded in Si₃N₄, mainly focused on the structural synthesis and the characterization of their photo-emission properties. For example, Lee *et al.* reported on elongated Ge nanocrystals synthesized by post-annealing of Ge-rich nitride/Si₃N₄ multilayers deposited by sputtering.¹⁹ However, contrasting results appear in the literature for the growth kinetics of QDs in SiO₂ or Si₃N₄ matrices. Recently, Chang *et al.* found an enhanced Ostwald ripening rate and an improved crystallinity of Ge QDs in Si₃N₄ synthesized by thermal oxidation of Si_{0.85}Ge_{0.15} layers deposited by low-pressure chemical vapor deposition (LPCVD) on Si₃N₄.²⁰ On the contrary, stoichiometric Si₃N₄ films implanted with Ge showed retarded QD ripening and crystallization kinetics with respect to Ge QDs in SiO₂ implanted with the same Ge dose.¹⁸ A significant role of the embedding matrix was also found for the optical bandgap of these systems, with Ge QDs in Si₃N₄ absorbing light more efficiently than in SiO₂.¹⁸ This effect, together with the lower tunneling barrier height offered by Si₃N₄, could potentially open a route toward the fabrication of efficient photodetectors and solar cells.

Although the use of Ge QDs in Si₃N₄ already showed interesting potential for application in QD-based memories,²¹ resonant-tunneling diodes,²² and thermoelectric devices,²⁰ no studies have been performed regarding the light harvesting and photo-carrier extraction mechanisms in devices employing Ge QDs in Si₃N₄. In particular, some open

^{a)}Author to whom correspondence should be addressed. Electronic mail: Salvatore.cosentino@ct.infn.it

questions concerning the use of Ge QDs in the fabrication of light harvesting devices remain. It is not well known whether the structural and optical properties of Ge QDs can be controlled by the embedding matrix and how this can affect the photo-conversion efficiency.

For these reasons, we present a detailed study on the synthesis and light absorption of Ge QDs embedded in Si₃N₄ and SiO₂ matrices produced by plasma enhanced chemical vapor deposition (PECVD). We found that the hosting matrix has a key-role in the kinetics of Ge QD growth, as well as in the optical absorption properties of these systems. Finally, Ge QDs embedded in Si₃N₄ are shown to play an active role in light detection in a photodetector realized for this purpose.

EXPERIMENTAL

Thin films containing Si:Ge:O or Si:Ge:N alloys (hereafter named SiGeO and SiGeN, respectively) have been deposited by PECVD on fused silica quartz or p-type Si substrates kept at 250 °C. Different Ge concentration have been obtained by varying the flux of GeH₄ while keeping constant the fluxes of SiH₄ and N₂O gases, used as precursors for the growth of SiGeO films. Instead of N₂O, NH₃ precursor was used for the deposition of SiGeN films. As deposited samples underwent thermal annealing in the 600–850 °C range in N₂ atmosphere to induce the phase separation of Ge in SiGeO and SiGeN alloys and the precipitation of excess Ge into nanoclusters (NCs). The presence and size distribution of Ge NCs, as well as the film thickness, were evaluated by cross sectional Transmission Electron Microscopy (TEM) analysis, using a JEOL 2010F TEM microscope at 200 kV in conventional dark field mode. We recognized the QDs according to the degree of overlap between QDs either by automatic particle identification software or manually by locating their boundaries. In the case of automatic identification, the spatial noise of the original micrograph is filtered by masking its Fast Fourier Transform (FFT), cutting off the high frequency component. The particles then are automatically recognized by standard computer processing, taking into account their contrast.²³ In this case, several hundred particles were measured. In the case of overlapping particles, this method does not produce good results, therefore a manual recognition of the QDs was required. For each sample, about one hundred of particles were analyzed, manually. For each set of data, we finally calculated the average size and the standard deviation.

The elemental composition of SiGeO and SiGeN films (as deposited or after thermal annealing) was determined by Rutherford backscattering spectrometry (RBS), using a 2.0 MeV He⁺ beam in random configuration and with a backscattered angle of 165° (spectra not shown). RBS spectra have been simulated using SIMNRA software to determine the Si, Ge, O, and N content and the stoichiometry of each film.²⁴ Small amounts of nitrogen (~5%) have been found in as deposited SiGeO samples (due to the use of N₂O gas), while oxygen contaminations (~10%) are present in SiGeN, probably due to absorption through the atmosphere. Micro Raman spectroscopy was performed by focusing the 488 nm

line of a cw Ar⁺ laser in an inverted microscope. The Raman spectra were collected with a high resolution monochromator and CCD camera system. Light absorption analysis was performed on samples deposited onto fused silica substrates. Normal transmittance (*T*) and the 20° reflectance (*R*) spectra in the 200 to 2000 nm wavelength range were acquired using a Varian Cary 500 double-beam scanning UV/visible/NIR spectrophotometer, as described in Ref. 15.

Ge NCs embedded in SiGeO and SiGeN alloys were used to fabricate prototypal photodetector devices. A metal-insulator-semiconductor (MIS) configuration was obtained by sputtering 500 nm thick In₂O₃:SnO₂ (ITO) contacts (circular shape, 0.5 cm² area) upon SiGeO (or SiGeN) films (as deposited or annealed) grown on p-Si substrate. Current density vs. voltage measurements have been performed in dark and under monochromatic illumination (400 to 1100 nm wavelength range) with a Keithley 4200 semiconductor characterization system.²⁴ The radiation source consists of a 250 W tungsten-halogen lamp coupled with a SP-2150 monochromator and a fiber bundle (19 individual optical fibers) to focus the light at different wavelengths on the sample placed within a Karl Suss probe station. The energy of the monochromatic radiation, power ~3 ÷ 10 μW, was monitored by an Ophir Nova II optometer.²⁵

RESULTS AND DISCUSSION

Table I summarizes the values of thickness (from TEM) and Ge content (from RBS) of as deposited and SiGeO and SiGeN films annealed at 800 °C. The value of GeH₄ flux (in sccm) was used as a suffix number to name the different samples. SiGeO films were around 400 nm thick, while SiGeN ones are almost half in thickness. Ge content in the as deposited films increases with the increasing of GeH₄ flux, from 8% to 16% for SiGeO films and from 13% to 22% in SiGeN films. Thermal annealing at 800 °C leads to thickness reduction and densification in both types of films, more pronounced for the SiGeO case. Ge content in the annealed samples increases from 10% to 17.5% in SiGeO and from 17% to 27% in SiGeN films with the GeH₄ flux, slightly increasing with respect to the corresponding values of as deposited films because of the preferential evaporation of N and H related species. Thermal annealing of SiGeO and SiGeN alloys induces nucleation and growth of small Ge precipitates^{20,26} embedded in SiO₂ and Si₃N₄ matrices, respectively.

TABLE I. Film thickness (extracted by TEM) and Ge content (extracted by RBS), before and after 800 °C annealing, for SiGeO and SiGeN films deposited on quartz by PECVD.

Samples	GeH ₄ flux (sccm)	Thickness (nm)		% Ge	
		As deposited	800 °C	As deposited	800 °C
SiGeO60	60	430	330	8	10
SiGeO90	90	365	280	12	15
SiGeO120	120	410	310	16	17.5
SiGeN45	45	180	170	13	17
SiGeN60	60	180	170	18	20
SiGeN90	90	200	150	22	27

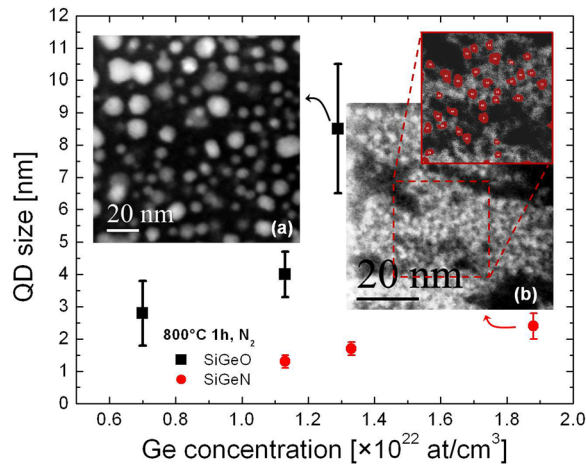


FIG. 1. Mean QD size as a function of the Ge atomic concentration in SiO_2 and Si_3N_4 films annealed at 800°C . The insets show two representative TEM images of Ge QDs in the SiGeO120 sample (a) and in the SiGeN90 sample (b).

We investigated the average size of QDs after 800°C annealing as a function of the Ge concentration in both types of matrices. The TEM images in the insets of Fig. 1 (SiGeO120 and SiGeN90 samples) reveal the presence of Ge QDs visible as bright spots (due to high Z-contrast of QDs with respect to matrix). We identify the QDs either by automatic particle identification software or manually by locating their boundaries according to the degree of overlap between QDs.²³ TEM analyses have been performed on all samples, allowing to report the QD size versus Ge content trend for both matrices. Ge QDs in SiGeO films exhibit a mean size growing from about 2.9 ± 1 nm to 8.5 ± 2 nm with increasing the Ge concentration from 0.7 to 1.3×10^{22} at/cm³. Despite the larger Ge concentration in SiGeN films (from $\sim 1.1 \times 10^{22}$ to 1.9×10^{22} at/cm³), here the QDs are much smaller and closely packed with respect to the case of SiGeO films. As shown in the inset (b) of Fig. 1, for SiGeN films, it is quite straightforward to identify particles of about 1–2 nm, considerably smaller than the average QD sizes measured in the SiGeO films (Fig. 1(a)).

As observed in the insets of Fig. 1, also a different QD packaging is present in the two matrices. In particular, by considering the QD mean size and assuming that after annealing all the Ge in excess in the alloy is fully involved in the QD nucleation, we can give a rough estimation of the average QD concentration. Surface-to-surface QD separation ($\langle a \rangle$) can be estimated as well. For SiGeO samples, QDs concentration ranges from $\sim 2.5 \times 10^{18}$ QD/cm³ ($\langle a \rangle \sim 4$ nm), for the sample with 10% Ge, to a value of 3×10^{17} QD/cm³ ($\langle a \rangle \sim 7$ nm), for the sample having 17.5% Ge. Annealing of SiGeN films produces a much more packed array of very small QDs, as shown in the inset of Fig. 1. In this case, a QD concentration of the order of $0.5\text{--}1 \times 10^{20}$ QD/cm³ is found, corresponding to a mean surface-to-surface distance below 1 nm, roughly independent of the Ge content. The so-estimated Ge QD density and $\langle a \rangle$ should be taken as upper values, since in CVD methods incomplete precipitation of excess Ge cannot be ruled out.^{15,27} The larger QD density and the limited growth of QD size in SiGeN films can be

accounted for by a low diffusivity of Ge atoms in SiGeN films grown by PECVD. The different atomic diffusivity of Ge among the two matrices can be related to different amount of structural defects involved in the mechanism of Ge diffusion. This point is further confirmed by previous observation of stoichiometric Si_3N_4 and SiO_2 matrices implanted with Ge.¹⁸ In that case, the lower diffusivity of Ge in Si_3N_4 (below 7×10^{-17} cm²/s at 850°C) compared with SiO_2 (of the order of 10^{-13} cm²/s at 800°C)²⁸ retarded the QD ripening in Si_3N_4 and led to the formation of a narrow size distribution (~ 2 nm) of Ge QDs in Si_3N_4 against a more sparse array of larger QDs (size $\sim 3\text{--}24$ nm) in SiO_2 . In this paper, a similar behavior occurs for PECVD SiGeO and SiGeN alloys, indicating a clear role of the embedding matrix in the nucleation and growth of Ge QDs.

Further confirmation of the different growth kinetics of Ge QDs in the two matrices comes from the normalized “as measured” Raman spectra reported in Fig. 2. In fact, it is well known that thermal annealing also induces a concomitant transition from the amorphous to the crystalline phase of Ge QDs.²⁹ In order to evaluate the extent of such transition for SiO_2 and Si_3N_4 matrix, we performed Raman analysis on samples annealed at different temperatures and with different content of Ge. Top panel [Fig. 2(a)] reports the Raman spectra of SiGeO90 sample before and after thermal annealing at 800 and 850°C . The broad band in the $240\text{--}290$ cm⁻¹ range of the as deposited film corresponds to the convolution of the TO and LO phonon modes in amorphous (a-) Ge.³⁰ After thermal annealing at 800°C , the appearance of a narrow peak centered at around 300 cm⁻¹ (TO phonon mode in crystalline (c-) Ge)³⁰ reveals partial transition to the crystalline phase of Ge in QDs. However, a substantial fraction of Ge QDs is still in the amorphous phase, as suggested by the

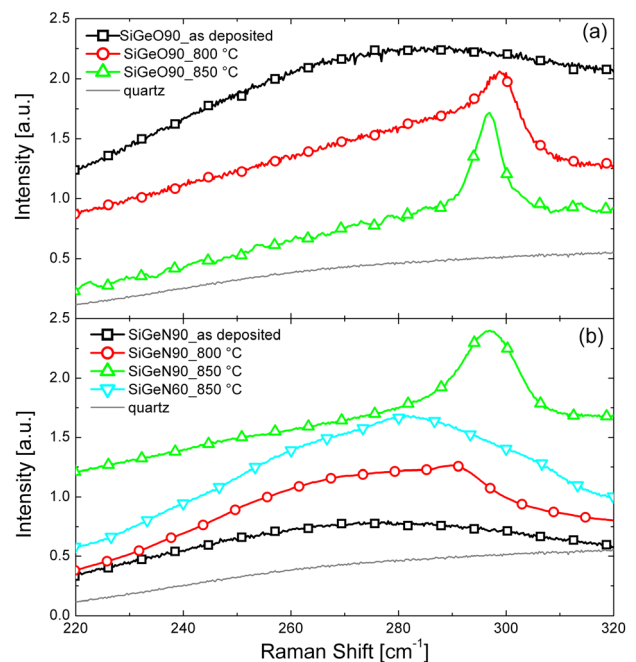


FIG. 2. Raman spectra of as deposited SiGeO (a) and SiGeN (b) films and evolution after thermal annealing at 800 and 850°C . The spectra of the fused silica substrate are reported for comparison, Raman spectra of all samples are vertically offset for clarity.

presence of the broad shoulder at 280 cm^{-1} . Only after a further increase of the annealing temperature to 850°C , complete crystallization of QDs occurs. On the contrary, only a limited crystallization occurs for Ge QDs in SiGeN films. Figure 2(b) reports the Raman spectra for SiGeN60 samples for which, despite the higher Ge concentration ($\sim 20\%$) and the high thermal budget provided after annealing at 850°C , most of Ge QDs remain in the amorphous phase, as pointed out by the broad band in the Raman spectra. Full crystallization of Ge QDs is observed only after annealing at 850°C in the Ge richest samples (with up to 27 Ge at. %). Therefore, an evident threshold of Ge concentration exists for the crystallization of Ge QDs in SiGeN films.

Very recently, retarded crystallization have been observed also for QDs in Ge-rich Si_3N_4 multilayers produced by magnetron sputtering, but with a very large threshold of ~ 50 Ge at. % for annealing at 900°C .¹⁹ Indeed, this limited crystallization can be accounted for by the larger interfacial energy between Ge and Si_3N_4 in comparison with SiO_2 , which requires a larger critical radius for Ge NC in Si_3N_4 .¹⁸ Thus, a clear role of the embedding matrix and Ge concentration emerges in the Ge NCs synthesis and crystallization, as the reduced mobility of Ge atoms in Si_3N_4 limits the cluster ripening and, as a consequence, also the QD crystallization.

Once the formation and growth of Ge QDs in the two CVD matrices is evaluated, the optical absorption properties were compared to determine the role of QD size and the effect of the matrix, if any, on the photon absorption mechanism. Fig. 3 reports the absorption coefficient spectra of as deposited and 800°C annealed SiGeO and SiGeN films for different Ge concentrations. The optical absorption spectrum of a 125 nm thick amorphous (a-) Ge film is also reported for comparison. Both SiGeO and SiGeN films display lower absorption coefficients with respect to a-Ge since the

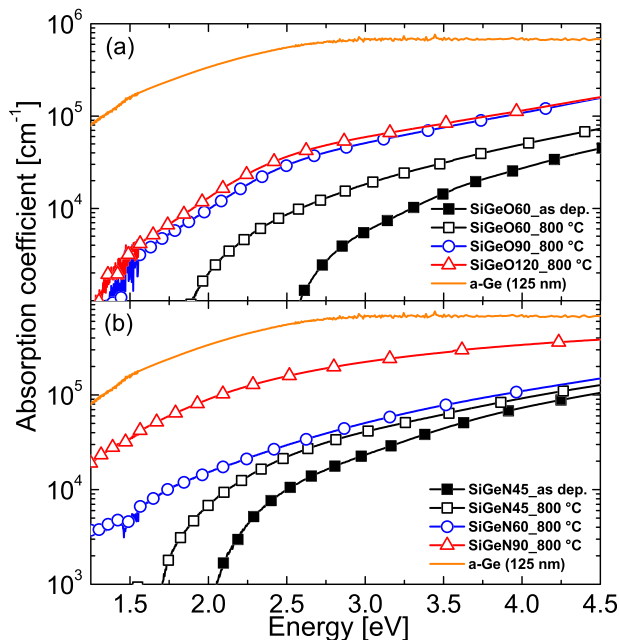


FIG. 3. Absorption coefficient spectra of as deposited (closed symbols) and 800°C annealed (open symbols) SiGeO (a) and SiGeN (b) films for different Ge concentration. The absorption coefficient of an unconfined Ge film (125 nm of thickness) is given for comparison.

majority of the films consists of an almost transparent matrix (SiO_2 or Si_3N_4), while only Ge atoms involved in the QDs formation (~ 10 to 20%) are responsible for the absorption process. As clearly shown in Fig. 3, thermal annealing has a strong role on the optical absorption of our samples and induces an evident increase of the absorption coefficient with a concomitant red-shift of the absorption energy onset. A similar trend occurs also when the Ge concentration is increased. In fact, increasing the Ge content within the films leads to a larger amount of Ge aggregates responsible for the absorption process, giving rise to a larger absorption coefficient. Moreover, increasing the Ge concentration also ensures the growth of larger QDs. This effect can partially account for the red-shift of the optical absorption spectra, in agreement with quantum confinement effects occurring in these systems. It is worthy of note that Ge QDs embedded in SiGeN films show a larger absorption coefficient when compared to those in SiGeO films. Moreover, they exhibit a considerably lower absorption energy onset despite their much smaller size.

To better clarify the role of the matrix and size on the light absorption in Ge QDs, we applied the Tauc model, describing the absorption process in bulk amorphous semiconductors, for the confined system studied here. Under the assumption of parabolic band edges and optical transitions between extended states from the valence band to the conduction band (usually valid for α values larger than $1 \times 10^4\text{ cm}^{-1}$), the energy dependence of α is satisfactorily modeled, by the Tauc law

$$\alpha = \frac{B}{h\nu} \left(h\nu - E_G^{\text{bulk}} \right)^2, \quad (1)$$

where $h\nu$ is the energy of the incoming photons, E_g is the optical bandgap and B is the Tauc coefficient, describing the efficiency of light absorption.^{31,32} If the Tauc law properly describes the light absorption also for our system, a plot of $(\alpha h\nu)^{1/2}$ versus $h\nu$ (called Tauc plot) would give a linear trend in the energy range for which $\alpha > 1 \times 10^4\text{ cm}^{-1}$. As shown in Fig. 4 for a selected set of samples, this is clearly what occurs for QDs grown after thermal annealing at 800°C (which are

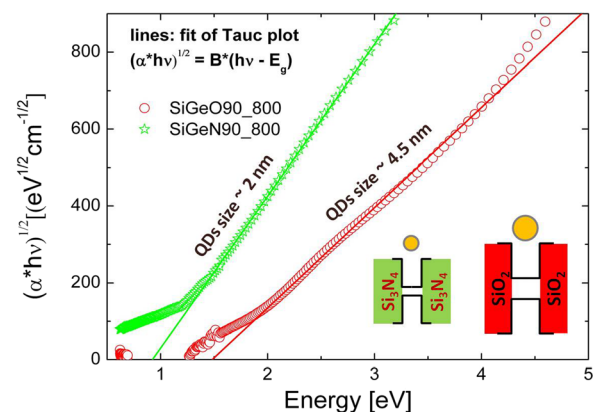


FIG. 4. Selected Tauc plot (symbols) and corresponding linear fits (lines) for Ge QDs produced after annealing at 800°C of SiGeO and SiGeN films. A schematic representation of the different confining barriers is also drawn in the figure.

in large part still in the amorphous phase) for both types of matrices. Thus, the photon absorption process described by the Tauc model is valid also for our confined system and allows us to determine E_g through a linear fitting procedure (lines in Fig. 4). By comparing the Tauc plots of Ge QDs embedded in Si_3N_4 or SiO_2 , as shown in Fig. 4, the role of the matrix clearly emerges. In fact, Ge QDs in Si_3N_4 evidence a lower bandgap than in SiO_2 matrix, despite their smaller size. This effect could be in agreement with the lower barrier height of Si_3N_4 (~ 5.3 eV) in comparison with SiO_2 that reduces the QCE. In fact, according to the theory, by reducing the height, V_0 , of the potential barriers a lower confinement of the electron-hole pair should occur and the value of E_g given is reduced by the factor $\left[1 + \frac{\hbar}{r\sqrt{2m^*V_0}}\right]^2$.^{5,18}

Symbols in Fig. 5 summarize the values of the optical bandgap for the two matrices, extracted with the Tauc plot method, as a function of the QD size. Ge QDs embedded in both types of matrices exhibit a clear size-dependent shift of E_g . In particular, Ge QDs in SiO_2 display a blue-shift of about 1 eV by shrinking the QD size down to 3–4 nm. A blue-shift of E_g occurs also for Ge QDs in Si_3N_4 , where E_g increases from about 0.9 eV (close to the E_g value of unconfined Ge, ~ 0.8 eV (Ref. 32)) for ~ 2 –3 nm QDs to a value of about 1.5 eV for slightly smaller QDs of 1–2 nm of diameter. In order to understand if these blue-shifts are related to quantum confinement effects, plots of the expected E_g curves for both finite and infinite potential barrier case have been plotted. E_g values for QDs in SiO_2 clearly follow the curve for the infinite barrier case. Therefore, the size dependent shift of E_g for Ge QDs in SiO_2 is mainly ascribed to QCE. For these samples, we fitted our E_g data within the effective mass theory according to the relationship: $E = E_g^{\text{bulk}} + A/D^2$, where E_g^{bulk} is the bandgap of a-Ge bulk and $A = \pi^2\hbar/2m^*$ (m^* reduced effective mass of excitons) is the confinement coefficient, being our only fitting parameter. In particular, we found a confinement coefficient of 11.7

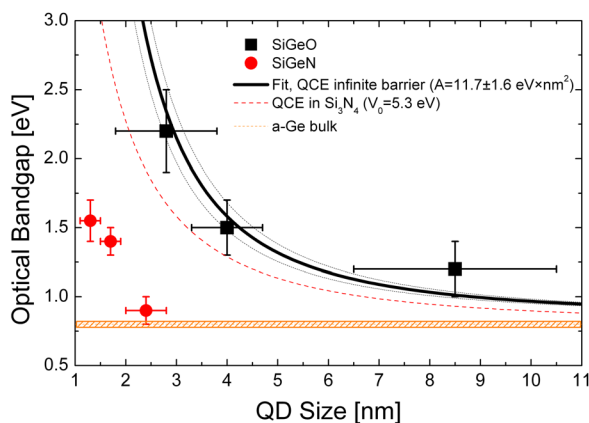


FIG. 5. Experimental values of the optical bandgap versus QD size of Ge QDs grown after thermal annealing at 800 °C of SiGeO (squares) and SiGeN (circles) films. The solid line was obtained through fitting from the effective mass theory for three-dimensionally confined a-Ge QDs in SiO_2 (infinite barrier case). Fitting error is reported as small dashed lines. The red dashed line represents the theoretical bandgap for QDs embedded in Si_3N_4 (finite barrier case). The horizontal bar represents the optical bandgap of unconfined a-Ge [30].

$\pm 1.6 \text{ eV} \times \text{nm}^2$, resulting in a very strong confinement for carriers in a-Ge QDs. Such a value is about 3 times larger than the A value ($4.35 \text{ eV} \times \text{nm}^2$) obtained for single a-Ge QW embedded in SiO_2 (Ref. 32) and is a further confirmation of the predominant role of quantum confinement effect in the optical absorption. In fact, such an increment of the confining parameter is fully in agreement with theory, since A is proportional to $1/m^* = 1/m_e^* + 1/m_h^*$ (where m_e^* and m_h^* are the electron and hole effective masses, respectively) and the effective masses are assumed to be isotropic for the three directions in amorphous materials. Therefore, the confinement coefficient for a-QDs is expected to be 3 times larger than for a-QW. In addition, in a-Si nanostructures, the A parameter was experimentally observed to increase by a factor of 3 going from 1D (QWs) to 3D (QDs) confinement by Park *et al.*³³ Recently, Barbagioanni *et al.* reported the values of A calculated using EMA approach for c-Si and c-Ge NS, giving an upper value of $7.88 \text{ eV} \times \text{nm}^2$ for Ge nanocrystals.³⁴ While these estimations better agree with experimental data for Si, some discrepancies appear for a-Ge QDs which experimentally show a confinement effect stronger than what theory predicts, probably related to a reduction of the effective mass in amorphous NS.³⁴

Even if the optical behaviour of our Ge QDs embedded in SiO_2 can be well modelled by quantum confinement theory, their optical bandgap in Si_3N_4 strongly deviates from a pure quantum confinement regime. In fact, though Ge QDs in Si_3N_4 show a clear size-dependent shift of E_g , this behaviour cannot be accounted for uniquely by quantum confinement which predicts larger values of shift. Actually, Ge QDs in Si_3N_4 can be affected by a large amount of disordered boundary regions or amorphous like shells due to their very small size. The lower experimental values of E_g with respect to a pure quantum confinement regime can be explained by optical transitions involving mid-gap states introduced by the presence of NC/matrix interfaces. This hypothesis is also in agreement with recent calculations on the effects of the strain and surrounding matrix on the optical bandgap of Si nanocrystals.¹³ The strain produced at the QD/matrix interface determines a red shift of the absorption spectra. In particular, for nanocrystals smaller than 2 nm, the proportion of atoms at the Si/ SiO_2 interface becomes relevant, producing surface-related states that may affect the quantum confinement appearing as inner band gap states and followed by a drastically change of their optical response.¹³ A similar mechanism can explain the large deviation of E_g in Ge QDs in Si_3N_4 with respect to quantum confinement law.

In order to test if photo-generated carriers in Ge QDs can be efficiently collected through the action of an external electric field E , we deposited a 500 nm thick ITO film (0.5 cm^2 circular area, $5.9 \text{ } \Omega/\text{sq}$ sheet resistance) on top of our SiGeO and SiGeN layers grown on p-doped Si, as illustrated in the schematic of Figure 6. We performed transversal current density versus voltage (J - V) measurements in the dark and under light conditions on this metal/insulator/semiconductor device, with the p -Si substrate grounded and the top contact swept from -5 V to 5 V . We reported in Figure 6 the J - E curves of the devices with Ge QDs in the two different matrices in order to properly compare the electrical

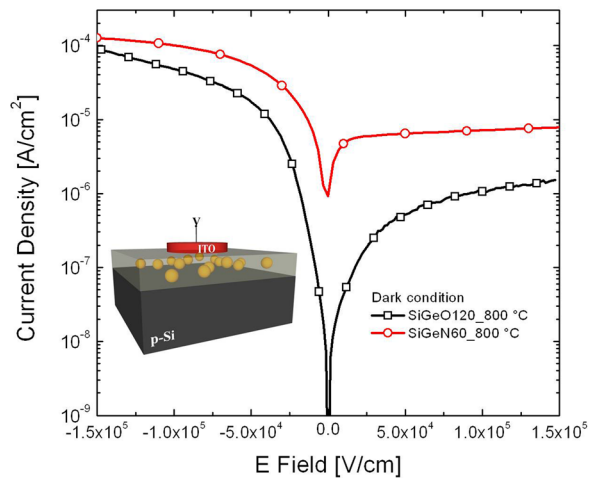


FIG. 6. J - E characteristics in dark condition of MIS devices with Ge QDs embedded in SiO_2 (SiGeO120_800) or Si_3N_4 (SiGeN60_800). The inset shows a schematic representation of the device structure.

conduction between films having different thicknesses, since the applied gate voltage mostly drops across the dielectric (SiO_2 or Si_3N_4) layers. Both kinds of devices show a rectifying behavior of the J - E characteristic, with a rectification ratio of ~ 100 at $\pm 1.5 \times 10^5$ V/cm for Ge QDs in SiO_2 and ~ 20 for QDs in Si_3N_4 . Similar characteristics have been previously reported for MIS structures containing Ge or Si QDs and attributed to a space-charge-limited mechanism of conduction.³⁵ The QD layer can be modeled as a three-dimensional resistance network in which all sites (Ge QDs) are connected by a finite tunneling barrier to its neighbors. As clearly shown in Figure 6, the MIS device with Ge QDs in Si_3N_4 exhibits a higher conduction. This behavior is in agreement with the lower barrier height offered by Si_3N_4 and also by the reduced QD-QD spacing that gives rise to a larger tunneling probability of carriers in respect to the more spaced array of QDs in SiO_2 . Hence, the conduction between dots can be significantly increased as the barrier height and QD spacing decrease, enhancing the collection of photo-generated carriers.

We performed photoresponse measurements in all samples. SiGeO ones did not show any significant differences between light and dark conditions. This can be due to the high potential barrier and to the larger film thickness offered by the SiGeO samples. For this reason, in the following, we present our best results obtained with the SiGeN samples containing 1.5 nm sized Ge QDs with a density of 6.5×10^{19} QD/cm³. As shown in Figure 7(a), upon illumination with white light the current density in forward bias remains largely unaffected, while it increases more than one order of magnitude in reverse bias. In addition, we observe also a clear wavelength dependence of the device in the 400–1100 nm range. In order to quantitatively investigate the spectral response of such kind of photodetector and clarify the role of Ge QDs, it is essential to relate the absorption properties to the photo-current behavior during illumination. To this aim, we calculated the spectral IQE, defined as the number of carriers collected at the output of the device per each absorbed photon at a given voltage.

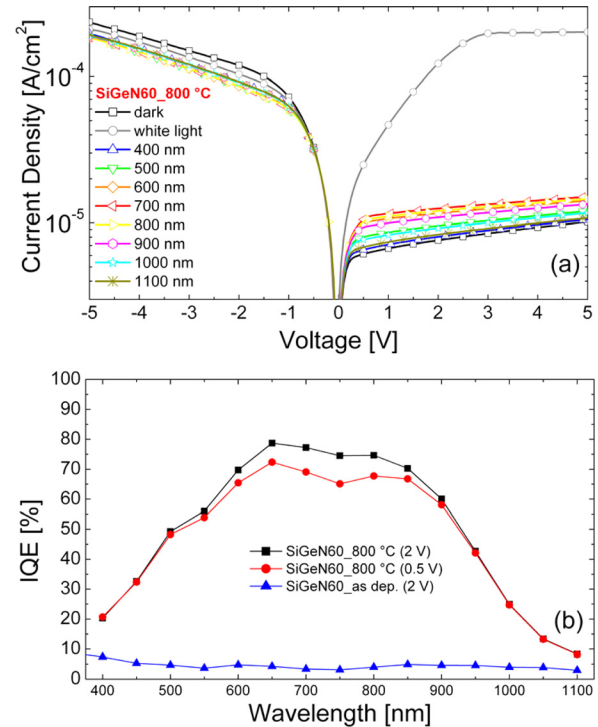


FIG. 7. J - V characteristics of the MIS photodetector in dark and as a function of the excitation λ in the 400–1100 nm range (a). Spectral IQE of MIS photodetector with Ge QDs embedded in Si_3N_4 at 0.5 V and 2 V of applied bias. The spectral IQE of a reference device without Ge QDs is given for comparison.

$$IQE = \frac{hc}{\lambda} \cdot \frac{(J_{light} - J_{dark})}{(1 - R) \cdot P}, \quad (2)$$

where P is the power of incident photons per unit area and R the fraction of light reflected by the device. As reported in Figure 7(b), the QD MIS device shows IQE values up to 70%–80% in the near infrared region when biased at 2 V and only slightly decreasing for a very low bias of 0.5 V. This means that almost all photo-generated electron-hole pairs can be extracted and collected under an external electric field E . On the contrary, the MIS device based on as deposited SiGeN layer shows only a low and flat photo-response in all investigated spectral ranges. This behavior indicates that annealing plays a key-role for QDs formation and electrical conductivity improvement. Therefore, Ge QDs in Si_3N_4 can be profitably used low-power consuming photodetectors or for light harvesting in proper designed PV cells. In order to explain the working mechanism, we consider the absorption spectrum of samples SiGeN60 after annealing at 800 °C. Part of incident light is absorbed in the Ge QD layer, while the remaining part by the Si substrate. So, the photocurrent is due to the electron-hole pairs photo-generated in the QD layer or in the Si substrate and extracted by the applied bias. As the device is reverse biased, holes are pushed into the p -Si substrate and electrons to the transparent electrode. The proposed mechanism has been successfully used for modeling photo-detection in layers of Ge QDs in SiO_2 synthesized by magnetron sputtering.³ In that case, substrate was n -type doped and device responsivity was larger.³ Even if the substrate doping changes or the QD embedding matrix is different, a clear role of Ge QDs as trapping centers for one

species of charge carriers comes out. Finally, it should be noted that, for PECVD materials reported in this paper, only QDs in Si_3N_4 display a marked photo-detection behavior, as QDs in SiO_2 grown by PECVD do not reveal significant activity under illumination. This can be related to the deviation of E_g from the QCE rule (Fig. 5), as the presence of QD/matrix interface states can play a role in decreasing the optical bandgap and in allowing carrier transport through the layer under illumination.

CONCLUSIONS

In conclusion, we presented an experimental investigation on the synthesis, structural analysis, light absorption, and detection of Ge QDs embedded in insulating matrices. Ge QDs embedded in SiO_2 or Si_3N_4 have been obtained after thermal annealing (up to 850°C) in N_2 atmosphere of SiGeO or SiGeN layer deposited by PECVD. QD size can be modulated in the 1–9 nm range, by varying the starting Ge concentration. However, a different kinetics of growth was observed between two types of matrices. When embedded in Si_3N_4 , Ge QDs are much smaller in size ($\sim 1\text{--}2$ nm) and closer to each other than in SiO_2 case. In addition, also the concomitant crystallization of Ge QDs due to thermal annealing is retarded in Si_3N_4 , depending also on the Ge content. This behavior can be related to the reduced diffusivity of Ge in Si_3N_4 and to the larger interfacial energy required for the QD growth. The optical absorption of Ge QDs increases with the Ge content in both SiGeN and SiGeO films, in agreement with the synthesis and growth of QDs and showing a clear size-dependence of E_g . In particular, the optical bandgap of Ge QDs in SiO_2 can be tuned with size in good agreement with effective mass theory predictions. A confining parameter of around $11.7\text{ eV} \times \text{nm}^2$ has been extracted for Ge QD in SiO_2 . E_g values of Ge QDs in Si_3N_4 deviate from a pure quantum confinement regime, probably because of QD/matrix interface states and stress particularly relevant for very small QDs. Finally, light harvesting through QD based photodetectors has been investigated, showing that Ge QDs in Si_3N_4 have significant photoresponse. In fact, prototypical photodetectors showed photoconduction with internal quantum efficiency of $\sim 70\%$ – 80% at biases as low as 0.5 V.

ACKNOWLEDGMENTS

The authors thank C. Percolla, S. Tati, and G. Panté (MATIS CNR-IMM) for expert technical assistance and S. Morawiec for ITO depositions. This work has been sponsored by bilateral CNR-TUBITAK project “Application of nanoporous Si and Ge nanostructures to advanced solar cells” (Grant No. 211T142) and in the framework of the project ENERGETIC PON00355_3391233.

¹L. Pavesi, L. Dal Negro, C. Mazzoleni, G. Franzò, and F. Priolo, *Nature* **408**, 440 (2000).

²J. Liu, M. Beals, A. Pomerene, S. Bernardis, R. Sun, J. Cheng, L. C. Kimerling, and J. Michel, *Nat. Photonics* **2**, 433–437 (2008).

- ³S. Cosentino, P. Liu, S. T. Le, S. Lee, D. Paine, A. Zaslavsky, D. Pacifici, S. Mirabella, M. Miritello, I. Crupi, and A. Terrasi, *Appl. Phys. Lett.* **98**, 221107 (2011).
- ⁴J. M. Shieh, Y. F. Lai, W. X. Ni, H. C. Kuo, C. Y. Fang, J. Y. Huang, and C. L. Pan, *Appl. Phys. Lett.* **90**, 051105 (2007).
- ⁵G. Conibeer, M. Green, E. Cho, D. Konig, Y. Cho, T. Fangsuwannarak, G. Scardera, E. Pink, Y. Huang, T. Puzzer, S. Huang, D. Song, C. Flynn, S. Park, X. Hao, and D. Mansfield, *Thin Solid Films* **516**, 6748 (2008).
- ⁶T. Tayagaki, N. Usami, W. Pan, Y. Hoshi, K. Ooi, and Y. Kanemitsu, *Appl. Phys. Lett.* **101**, 133905 (2012).
- ⁷Y. M. Niquet, G. Allan, C. Delerue, and M. Lannoo, *Appl. Phys. Lett.* **77**, 1182 (2000).
- ⁸C. Bulutay, *Phys. Rev. B* **76**, 205321 (2007).
- ⁹S. Das, R. K. Singha, A. Dhar, S. K. Ray, A. Anopchenko, N. Daldosso, and L. Pavesi, *J. Appl. Phys.* **110**, 024310 (2011).
- ¹⁰P. Liu, S. Cosentino, S. T. Le, S. Lee, D. Paine, A. Zaslavsky, D. Pacifici, S. Mirabella, M. Miritello, I. Crupi, and A. Terrasi, *J. Appl. Phys.* **112**, 083103 (2012).
- ¹¹N. Usami, W. Pan, T. Tayagaki, S. T. Chu, J. Li, T. Feng, Y. Hoshi, and T. Kiguchi, *Nanotechnology* **23**, 185401 (2012).
- ¹²M. Zacharias and P. M. Fauchet, *Appl. Phys. Lett.* **71**, 380 (1997).
- ¹³R. Guerra, I. Marri, R. Magri, L. Martin-Samos, O. Pulci, E. Degoli, and S. Ossicini, *Phys. Rev. B* **79**, 155320 (2009).
- ¹⁴S. Cosentino, S. Mirabella, M. Miritello, G. Nicotra, R. Lo Savio, F. Simone, C. Spinella, and A. Terrasi, *Nanoscale Res. Lett.* **6**, 135 (2011).
- ¹⁵S. Mirabella, R. Agosta, G. Franzò, I. Crupi, M. Miritello, R. Lo Savio, M. A. Di Stefano, S. Di Marco, F. Simone, and A. Terrasi, *J. Appl. Phys.* **106**, 103505 (2009).
- ¹⁶C. Uhrenfeldt, J. Chevallier, A. N. Larsen, and B. B. Nielsen, *J. Appl. Phys.* **109**, 094314 (2011).
- ¹⁷S. Mirabella, S. Cosentino, M. Failla, M. Miritello, G. Nicotra, F. Simone, C. Spinella, G. Franzò, and A. Terrasi, *Appl. Phys. Lett.* **102**, 193105 (2013).
- ¹⁸S. Mirabella, S. Cosentino, A. Gentile, G. Nicotra, N. Piluso, L. V. Mercaldo, F. Simone, C. Spinella, and A. Terrasi, *Appl. Phys. Lett.* **101**, 011911 (2012).
- ¹⁹S. Lee, S. Huang, G. Conibeer, and M. Green, *J. Cryst. Growth* **383**, 36 (2013).
- ²⁰J. E. Chang, P. H. Liao, C. Y. Chien, J. C. Hsu, M. T. Hung, H. T. Chang, S. W. Lee, W. Y. Chen, T. M. Hsu, T. George, and P. W. Li, *J. Phys. D: Appl. Phys.* **45**, 105303 (2012).
- ²¹C. Tu, T. Chang, P. Liu, H. Liu, S. Sze, and C. Chang, *Appl. Phys. Lett.* **89**, 162105 (2006).
- ²²K.-H. Chen, C.-Y. Chien, and P.-W. Li, *Nanotechnology* **21**, 055302 (2010).
- ²³G. Nicotra, R. A. Puglisi, S. Lombardo, C. Spinella, M. Vulpio, G. Ammendola, M. Bileci, and C. Gerardi, *J. Appl. Phys.* **95**, 2049 (2004).
- ²⁴M. Mayer, “SIMNRA user’s guide,” Report No. IPP 9/113, Max-Planck-Institut für Plasmaphysik, Garching, 1997.
- ²⁵G. G. Scapellato, M. Rubino, I. Crupi, S. Di Marco, F. Simone, and S. Mirabella, *J. Appl. Phys.* **114**, 053507 (2013).
- ²⁶A. Rodriguez, T. Rodriguez, J. Sangrador, B. Morana, A. Kling, and C. Ballesteros, *Semicond. Sci. Technol.* **25**, 045032 (2010).
- ²⁷G. Franzò, M. Miritello, S. Boninelli, R. Lo Savio, M. G. Grimaldi, F. Priolo, F. Iacona, G. Nicotra, C. Spinella, and S. Coffa, *J. Appl. Phys.* **104**, 094306 (2008).
- ²⁸Y. Maeda, *Phys. Rev. B* **51**, 1658 (1995).
- ²⁹W. K. Choi, V. Ng, S. P. Ng, H. H. Thio, Z. X. Shen, and W. S. Li, *J. Appl. Phys.* **86**, 1398 (1999).
- ³⁰D. Bermejo and M. Cardona, *J. Non-Cryst. Solids* **32**, 405 (1979).
- ³¹J. Tauc, in *Amorphous and Liquid Semiconductors*, edited by J. Tauc (Plenum, New York, 1974), p. 175.
- ³²S. Cosentino, M. Miritello, I. Crupi, G. Nicotra, F. Simone, C. Spinella, A. Terrasi, and S. Mirabella, *Nanoscale Res. Lett.* **8**, 128 (2013).
- ³³N. M. Park, C. J. Choi, T. Y. Seong, and S. J. Park, *Phys. Rev. Lett.* **86**, 1355–1357 (2001).
- ³⁴E. G. Barbagiovanni, D. J. Lockwood, P. J. Simpson, and L. V. Goncharova, “Quantum confinement in Si and Ge nanostructures,” *J. Appl. Phys.* **111**, 034307 (2012).
- ³⁵A. I. Chou, K. Lai, K. Kumar, P. Chowdhury, and J. C. Lee, *Appl. Phys. Lett.* **70**, 3407 (1997).